NATURALISTA CAMPANO
ISSN: 1827-7160
Volume 28 Issue 1, 2024

Formulation and Evaluation of Allicin Loaded Nanosponges

Dr. Amol U. Gayke[1*], Ms. Pranali. K. Gadakh[2], (Associate Professor) Dr Dattatray M Shinkar[3], Prof. Preetam L. Nikam[4], Ms. Bharti. S. Garale[5], Prof. Vikas S. Shinde[6], Dr. Pradyumna Ige[7]

[1*,2,3,4,5,6,]Department of Pharmaceutics SND College of Pharmacy, Babhulgaon, Yeola, Dist. Nashik 423201

Corresponding Author: [1*]Dr. Amol U. Gayke
[1*]SND College of Pharmacy, Babhulgaon, Yeola, Dist. Nashik 423201
Email ID: amolgayke6687@gmail.com, Preetamnikam25@gmail.com

Abstract: Background: Fungal infections pose a significant health concern due to their prevalence and increasing resistance to conventional antifungal agents. Allicin, a sulfur-containing compound derived from garlic, exhibits potent antifungal properties. This study aimed to develop a nanosponge-loaded gel formulation of allicin for topical application to enhance its stability and efficacy. **Methods:** Allicin-loaded nanosponges were prepared using a crosslinking method, and the resulting formulation was characterized for particle size, zeta potential, and entrapment efficiency. Solubility analysis was conducted in various solvents, and the thermal behavior was assessed using Differential Scanning Calorimetry (DSC). Fourier Transform Infrared Spectroscopy (FTIR) was employed to investigate drug-excipient interactions. Optimization of the formulation was performed using a central composite design. In-vitro release studies and antifungal activity assays were conducted to evaluate the formulation's performance. **Results:** The optimized formulation, PF7, exhibited a particle size of 273.5 nm, zeta potential of -15.3 mV, and entrapment efficiency of 82.4%. Allicin showed higher solubility in ethanol (9.83±0.67 mg/mL) compared to water (5.89±0.77 µg/mL). FTIR and DSC analyses confirmed the stability and compatibility of allicin with the excipients. The in-vitro release studies demonstrated a controlled release profile with PF7 achieving 95.57% release over 12 hours. The nanosponge-loaded gel (GF) showed substantial antifungal activity with inhibition zones of 23.5±0.87 mm against Candida albicans and 24.4±1.23 mm against Aspergillus niger, comparable to the marketed standard. **Conclusion:** The nanosponge-loaded gel formulation of allicin demonstrated enhanced stability, controlled release, and effective antifungal activity, presenting a promising alternative for the treatment of topical fungal infections.

Keywords: Allicin, Nanosponges, Topical gel, Fungal infections, Antifungal activity, Controlled release, Drug formulation.

1. Introduction

Fungal infections are a significant health concern, affecting millions of people worldwide.[1] These infections range from superficial conditions such as athlete's foot and ringworm to more severe systemic infections that can be life-threatening, particularly in immunocompromised

individuals.[2] The prevalence of fungal infections has been rising, driven by factors such as increased use of immunosuppressive therapies, widespread use of antibiotics, and a growing population of individuals with chronic diseases.[3] Despite the availability of various antifungal agents, the emergence of drug-resistant fungal strains poses a considerable challenge to effective treatment.[4] Resistance to antifungal medications, such as azoles and echinocandins, is becoming increasingly common, necessitating the development of novel therapeutic strategies.[5]

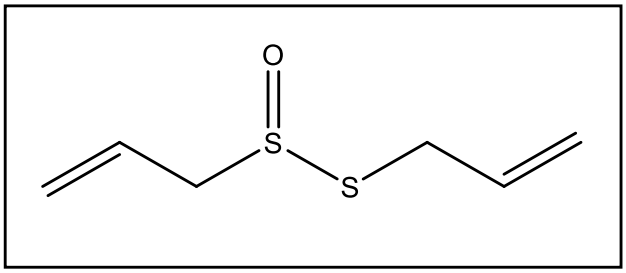

Figure 1: Structure of Allicin

Allicin, a sulfur-containing compound (Figure 1) derived from garlic (*Allium sativum*), has garnered significant attention for its potent antimicrobial properties.[6] Allicin is produced when garlic is crushed or chopped, converting alliin into allicin through the action of the enzyme alliinase.[7] This compound exhibits a broad spectrum of antimicrobial activity, including antibacterial [8], antiviral, and antifungal effects.[9] Allicin's antifungal potential has been well-documented [10], with studies demonstrating its efficacy against a variety of fungal pathogens, including Candida species and dermatophytes.[11] Its mechanism of action involves disrupting the cell membrane integrity of fungal cells, leading to cell death. Given its natural origin and potent antifungal activity, allicin represents a promising candidate for the development of new antifungal therapies [12].

Nanosponges are a novel class of nanoparticulate carriers that have shown great promise in drug delivery systems due to their unique structural and functional properties.[13] These tiny, porous particles are capable of encapsulating a wide range of therapeutic agents, protecting them from degradation, and facilitating controlled and sustained release.[14] Nanosponges are typically composed of biodegradable polymers [15], such as cyclodextrins or hyper-crosslinked polymers, which form a three-dimensional network with numerous cavities [16]. These cavities can efficiently entrap hydrophilic and hydrophobic drugs, enhancing their solubility, stability, and bioavailability [17]. Additionally, the high surface area and tunable surface chemistry of nanosponges allow for targeted delivery and improved penetration into biological tissues, making them particularly suitable for topical applications [18]. Their ability to release the encapsulated drug in response to specific stimuli further enhances their potential in precision medicine [19].

The objectives of the current research are to develop and fabricate a nanosponge-loaded gel formulation of allicin for the treatment of topical fungal infections. This study aims to explore the potential of nanosponges as a delivery system to enhance the stability and efficacy of allicin. Specifically, we seek to evaluate the formulation's physicochemical properties, assess its antifungal activity against common fungal pathogens, and determine its safety and effectiveness in topical application. Through this research, we hope to provide a novel and

effective therapeutic option for managing fungal infections, addressing the challenges posed by drug resistance, and leveraging the natural antifungal properties of allicin.

2. Materials and Methods

2.1. Materials

The Itraconazole was obtained from Sciquaint Innovations (OPC) Private Limited in Pune, India. The supplier of Poloxamer 188 was Research Lab Fine Chem Industries, located in Mumbai, India. We bought the oleic acid and Precirol® ATO 5 from Pure Chemical India Pvt. Ltd. in Pune, India. All solvents and chemicals used were of the analytical grade.

2.2. Methods

2.2.1. Calibration Curve of Allicin

The calibration curve for allicin was established by scanning solutions of varying concentrations (from 1 to 6 ppm) within a range of 800 to 200nm in the spectrum mode of a UV-Visible spectrophotometer. From this scanning process, the absorbance maximum was selected. The absorbance of the solutions from 1 ppm to 6 ppm was measured using a Shimadzu double beam UV-spectrophotometer in photometric mode, with ethanol serving as a reference blank. The absorbance maxima were identified through the carried-out procedure, and from these, the spectrum was formed.[20] The absorbance maxima were observed at 241nm, thus providing a basis for the calibration curve.

2.2.2. Solubility Analysis

Allicin was added in excess to 2 ml of ethanol, water, DMSO, and Phosphate Buffer pH 6.8 individually in 5-mL stopper vials with a capacity of 5, and the mixture was vortexed to ascertain the solubility of allicin in different organic solvents. After that, the mixture vials were placed in an orbital shaker and kept at 25±1.0 °C for 72 hours to reach equilibrium. After the samples had stabilized, they were taken out of the shaker and centrifuged for 15 minutes at 3,000 rpm. A membrane filter measuring 0.22 µm was used to filter the supernatant. The UV spectrophotometer was used to measure the allicin concentration at 241 nm.[21]

2.2.3. Determination of Melting Point

The melting point of the isolated Allicin was filled in the capillary tube which was sealed at one end. A similar procedure was followed for reference standard too. The capillary tubes containing the samples were placed in the Veego melting point apparatus and the instrument was switched on.[22] The temperature at which the samples melted was noted.

2.2.4. Fourier transform infrared (FTIR) spectroscopy.

The FTIR spectra of pure drug (Allicin) and Allicin + Excipients of NS were recorded and interpreted for the possible chemical interactions. The transparent pellets of these samples were prepared by mixing each of these components with potassium bromide and FTIR spectras were recorded in the region of 4000–400 cm^{-1} ‘‘(FTIR Spectrophotometer, Jasco Japan) [23].

2.2.5. Differential scanning calorimetry (DSC)

Thermal peaks of pure drug (Allicin) and Allicin + Excipients were evaluated for drug encapsulation. The samples (5 mg) were enclosed in aluminum pan and heated at a rate of 10

C/min in the temperature range of 30–300ºC, the device was purged with inert N2 gas at flow rate 20 mL/min "(Scinco N650, made in Italy)" during the study.

2.2.6. Experimental Design

A Central composite design of nine formulations were used formulation, The independent variables used will numeric factors namely, X1 - concentration of Polyvinyl alcohol [24] and X2 concentration of Ethyl cellulose [25]. The responses selected for statistical optimization will, R1- Entrapment efficiency and R2- Particle size as presented in Table 1 and 2.[26]

Table 1: Layout of Two Factor Three Level Design

Independent Variables				
Factors	**Coded Values**		**Actual Values (mg)**	
X1- Polyvinyl alcohol	-1	+1	600	1200
X2 - Ethyl cellulose	-1	+1	400	600
Dependent Variables (Response)				
R1- Entrapment efficiency (%)				
R2- Particle size (nm)				

Table 2: Allicin loaded Nanosponges compositions.

Batch code	**Composition**								
	PF1	**PF2**	**PF3**	**PF4**	**PF5**	**PF6**	**PF7**	**PF8**	**PF9**
Allicin (mg)	24.32	24.32	24.32	24.32	24.32	24.32	24.32	24.32	24.32
Polyvinyl alcohol (mg)	600	900	1324.26	1200	1200	475.73	900	900	600
Ethyl cellulose (mg)	400	641.42	500	400	600	500	500	358.57	600
Pluronic F68 (mg)	200	200	200	200	200	200	200	200	200
Dichloromethane (mL)	30	30	30	30	30	30	30	30	30
Distilled Water	q.s. to 100	q.s. to 100	q.s. to 100	q.s. to 100	q.s. to 100	q.s. to 100	q.s. to 100	q.s. to 100	q.s. to 100

2.2.7. Preparation of Allicin Nanosponges

Allicin nanosponges were prepared by different proportions of ethyl cellulose, polyvinyl alcohol and Pluronic F68 by emulsion solvent diffusion technique.[27] The disperse phase consisting of 800 mg Allicin and specified quantity of ethyl cellulose (Table 2) dissolved in 30 mL of dichloromethane was slowly added to a definite amount of PVA in 100 mL of aqueous continuous phase. The mixture was stirred at 1000 rpm on a magnetic stirrer for two hours.[26] The formed Allicin nanosponges were collected by vacuum filtration and dried in an oven at 40ºC for 24 h.

2.2.8. Preparation of NS loaded Gel for Optimized batch of NS.

Carbopol 940 (1% w/v) was added in small amounts to nanosponges (equivalent to 24.32mg) and continuously stirred with a mechanical overhead stirrer at 400 rpm. The carbopol

dispersion was fully dispersed and then neutralized to pH 7.0 with triethanolamine. and Spreadability, viscosity, and pH of the resulting gel were assessed.[28]

2.2.9. Evaluation of the NS formulation

2.2.9.1. Particle characterization

The particle size analysis of BTF loaded NS (BNS1-BNS4) was performed by using ‘‘Malvern Zetasizer NanoZS (Malvern Instruments, UK)”. The sample under investigation was diluted with distilled water (1: 200) and filled in disposable polystyrene cuvette. Measurement of particle size was done based on the dynamic light scattering (DLS) theory. All the samples were tested in triplicate (n = 3).[23]

2.2.9.2. Zeta potential

The zeta potential was measured for the determination of the movement velocity of the particles in an electric field and the particle charge. In the present work, the nanosponges was diluted 10 times with distilled water and analyzed by Zetasizer using Laser Doppler Micro electrophoresis (Zetasizer nano ZS, Malvern instruments Ltd., UK) [29].

2.2.9.3. Entrapment efficiency (%)

UV spectrophotometric method was used to estimate entrapment efficiency of allicin nanosponges. A calibration curve was plotted for Allicin in ethanol in the range of 1-6 µg/mL (Beer’s Lambert’s range) at 241 nm. 100 mg of allicin nanosponges of each batch were selected, powdered in a mortar and placed in 100 mL of methanolic HCl. Allicin was extracted by centrifuging at 1000 rpm for 30 min, filtered and analyzed concentration from calibration curve data after necessary dilution. Percentage entrapment was calculated as follows [30]:

$$\% EE = \frac{= Actual\ drug\ content\ in\ the\ NS}{Theoretical\ drug\ content} \times 100 \qquad (1)$$

2.2.10. Characterization of Prepared NS loaded Gel formulation.

2.2.10.1. pH Determination

The crucial test, particularly for the topical formulation, is pH assessment. The gel should have a pH of five to seven to resemble the state of skin. The prepared gel could irritate the patient if its pH is basic or acidic. I used an ELICO LI 613 digital pH metre to measure the pH of the prepared gel. The glass electrode was dipped into a gel after 1 gramme of gel was dissolved in 100 millilitres of distilled water and left for two hours. Every formulation had its pH measured three times, and averages were determined [31].

2.2.10.2. Spreadability

The spreadability of the gel formulations loaded with NS was assessed by a modified slide technique. A glass slide containing a tiny amount of NS loaded gel was topped with another slide. After five minutes of bearing a one kilogramme weight on the upper slide, the slide was raised, and a Vernier caliper was used to measure the diameter of the spread NS loaded gel in both directions. The spreadability was computed by the following formula [32]:

$$S = M.L/T$$

Where, M= weight tied to upper slide (10g); L = length of glass slide (6.8cm); T = Time taken to separate the slides

2.2.10.3. Viscosity

The viscosities of NS loaded gel formulations were measured using a brook field viscometer with spindle number 04. Once the spindle was lowered perpendicularly into the gel formulation's center in a beaker, being careful not to touch the bottom, it was spun at 2.5 rpm for five minutes. Notated was the viscosity reading [33].

2.2.11. *In-Vitro* Antifungal activity

The allicin, GF (NS (PF7) loaded gel) and marketed standard (MS) were subjected to *in-vitro* antifungal activity assessment against *Candida albicans* and *Aspergillus niger*. This was conducted using the microdilution technique [34]. The microbes were cultivated in Sabouraud dextrose broth and incubated for 24 hours at a temperature of 37°C. After incubation, the culture was diluted to achieve a concentration of 1 × 106 colony-forming units per milliliter (CFU/mL). The microdilution plates were prepared by inoculating each well with 100 µL of the fungal suspension and 100 µL of the respective compound dilution [35]. This procedure ensured a final concentration of the fungal suspension in each well of 0.5 × 106 CFU/mL. Fungiwin Cream was utilized as a positive control, while Dimethyl Sulfoxide (DMSO) served as the negative control. Following this setup, the plates were incubated at 37°C for another 24 hours.

2.2.12. Statistical Analysis

The data obtained from the experiments were analyzed using Design Expert software Expert® DX 13.0 (StatEase Inc., MN). Analysis of variance (ANOVA) was performed to determine the significance of the factors, and the effects of the factors on the dependent variables were presented using response surface plots.

3. Results and Discussion

3.1. Calibration of curve of Allicin

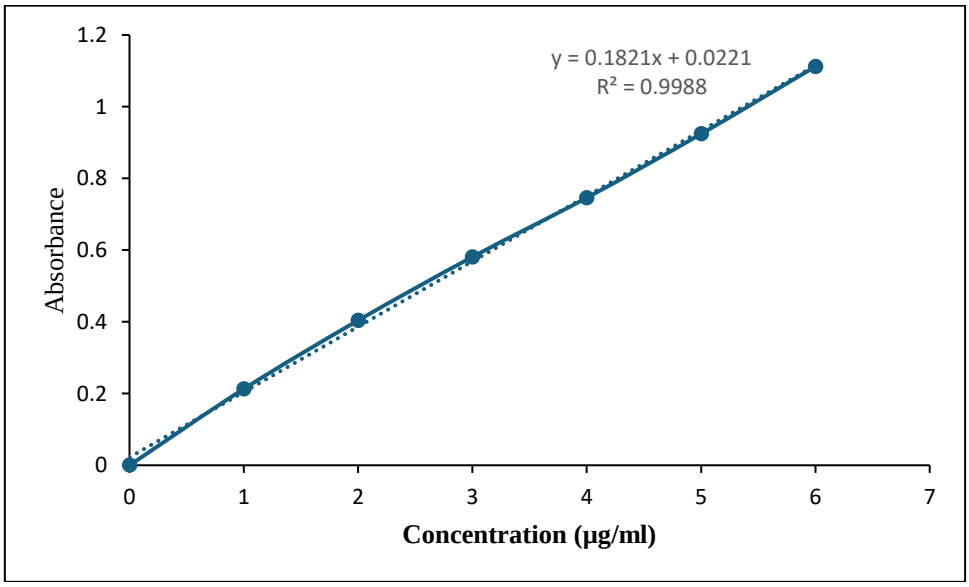

Figure 2: Calibration curve of Allicin in ethanol

The calibration curve of Allicin, as shown in Figure 2, presents a linear relationship between concentration and absorbance across the range tested (1 to 6 µg/ml). This linearity is substantiated by a high correlation coefficient (r^2) of 0.9976, indicating excellent agreement with Beer's Law which posits that absorbance should be directly proportional to concentration within this range. The slope of 0.0164 and intercept of 0.1203 further validate the consistency and reliability of the method used for determining Allicin's concentration. The progression of absorbance values from 0.213 at the lowest concentration to 1.112 at the highest confirms the assay's ability to differentiate effectively between different concentrations of Allicin, reinforcing its potential applicability in analytical and quality control settings.

3.2. Solubility analysis

Table 3: Results of solubility analysis of Allicin

Sr. No.	Solvent	Solubility	Results
1	Water	5.89±0.77 µg/mL	Slightly soluble
2	Ethanol	9.83±0.67 mg/mL	Freely soluble
3	Chloroform	8.43±0.68 mg/mL	Freely soluble
4	Phosphate Buffer pH 6.8	7.54±0.54 mg/mL	Freely soluble

Values are given mean, (n=3)

The solubility analysis of Allicin across various solvents, as presented in Table 3, reveals significant insights into the solubility profile of the compound, which is critical for its formulation and therapeutic application. Allicin demonstrates a stark contrast in solubility between aqueous and organic solvents. Specifically, in water, Allicin shows a solubility of only 5.89±0.77 µg/mL, classifying it as slightly soluble. This low solubility in water may pose challenges for formulations that require aqueous solutions, influencing its bioavailability and effectiveness in such preparations. Conversely, Allicin's solubility in ethanol, chloroform, and phosphate buffer pH 6.8 is significantly higher, recorded at 9.83±0.67 mg/mL, 8.43±0.68 mg/mL, and 7.54±0.54 mg/mL, respectively, all classified as freely soluble. These results suggest that Allicin is considerably more compatible with organic solvents and certain buffered systems, which could be advantageous in developing non-aqueous formulations such as tinctures, topical solutions, and injectables where higher solubility is beneficial for dose accuracy and therapeutic efficacy. The notably higher solubility in these solvents compared to water underscores the importance of selecting appropriate solvent systems for Allicin-based formulations to enhance drug delivery and activity

3.3. Melting point

Table 4: Melting point of Drug

Drug Name	Allicin	
Melting Point (ºC)	Standard	Observed
	24ºC-27ºC	25ºC-28ºC

The melting point of Allicin, as detailed in Table 4, presents a crucial characteristic of the drug that is pertinent to its storage, stability, and formulation. The standard melting point range for Allicin is given as 24ºC to 27ºC, which is closely matched by the observed melting point range of 25ºC to 28ºC. This slight variation in the observed range may be attributed to experimental

conditions or minor impurities, but it remains within a close proximity to the expected values, indicating the purity and consistency of the Allicin sample used

3.4. Results of FTIR Analysis

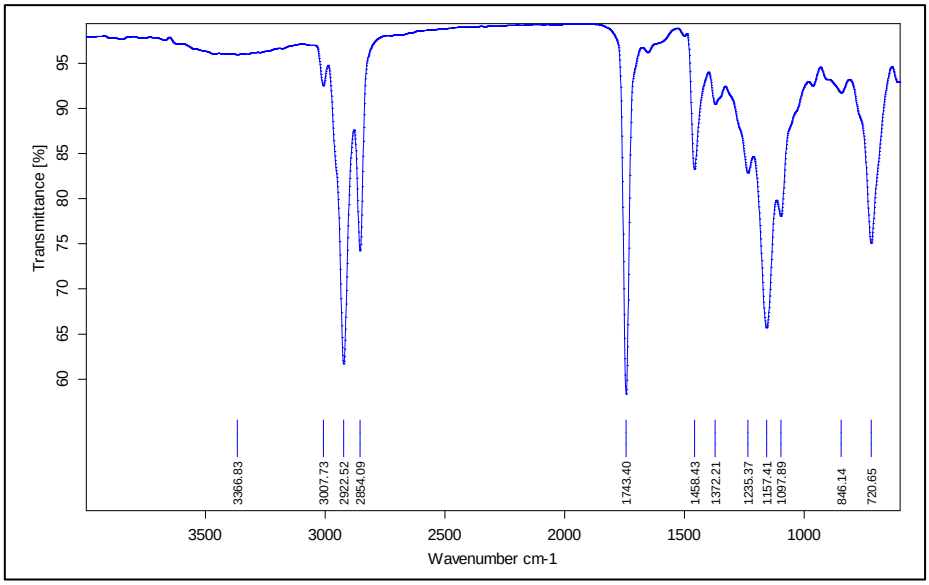

Figure 3: FTIR spectra of Allicin

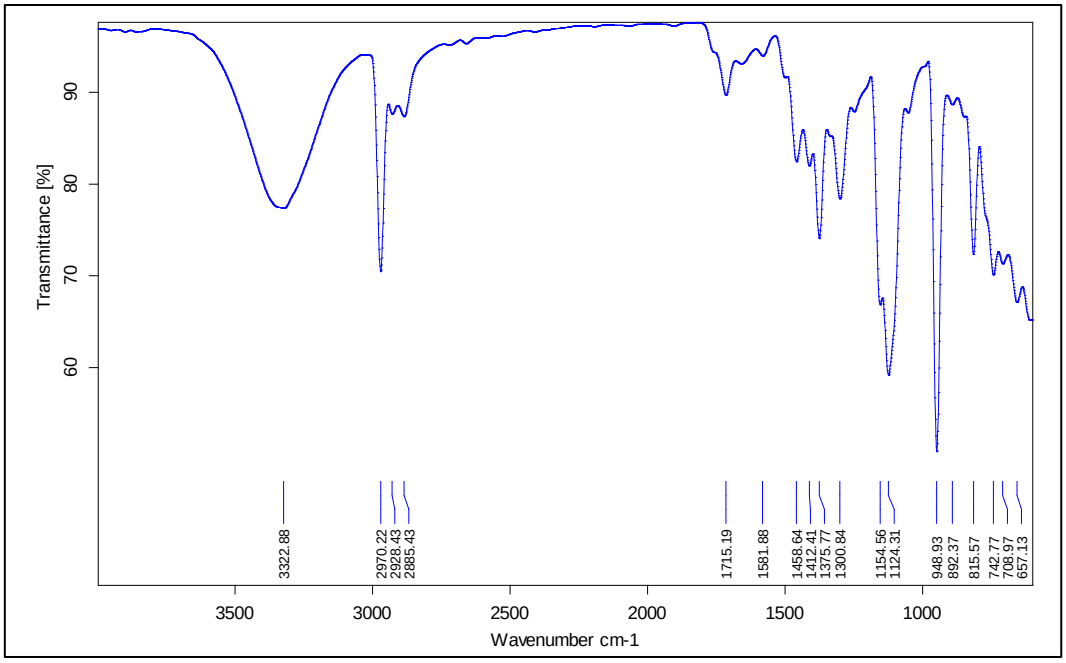

Figure 4: FTIR spectra of Allicin + Excipients

The Fourier Transform Infrared Spectroscopy (FTIR) results provide a detailed look into the chemical interactions, if any, between Allicin and the excipients used. The FTIR spectra, as shown in Figures 3 and 4, help to identify any significant shifts or alterations in the functional group peaks, which could indicate chemical incompatibilities between the drug and the excipients. In the case of Allicin, the FTIR spectrum exhibits specific peaks associated with its

functional groups. The O-H stretch observed at 3366.83 cm^{-1} in pure Allicin shifts to 3322.88 cm^{-1} in the Allicin-excipient mixture, indicating a slight change in hydrogen bonding possibly due to physical interactions with the excipients. The C-H stretch and C=O stretch are other critical indicators, seen at 3007.73 cm^{-1} and 1743.40 cm^{-1} respectively in pure Allicin, shifting to 2970.22 cm^{-1} and 1715.19 cm^{-1} in the mixture. These shifts are minor and typical in pharmaceutical formulations, suggesting altered environmental conditions around these groups. The peaks such as the C=C stretch and C-H bending show very minimal changes (1458.43 to 1458.64 cm^{-1} and 1372.21 to 1375.77 cm^{-1}, respectively), supporting the stability of the aromatic and aliphatic structures in Allicin when mixed with excipients. However, notable shifts like the S=O stretch from 1235.37 cm^{-1} in pure Allicin to 1300.84 cm^{-1} in the mixture may indicate some interaction at the sulfur-containing groups, though such a change could also stem from physical alterations rather than a direct chemical interaction. The -CH_2 rock shows a noticeable shift from 846.14 cm^{-1} to 815.57 cm^{-1}, which might suggest changes in the molecular environment possibly due to excipient interaction.

3.5. Results of DSC Analysis

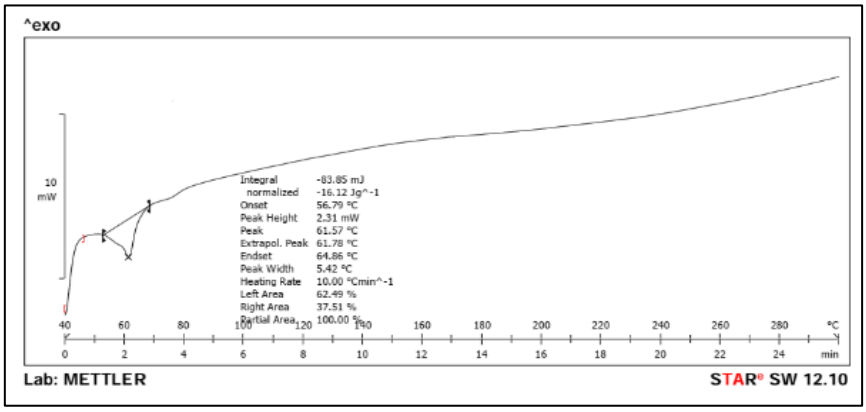

Figure 5: DSC Spectra of Pure Drug (Allicin)

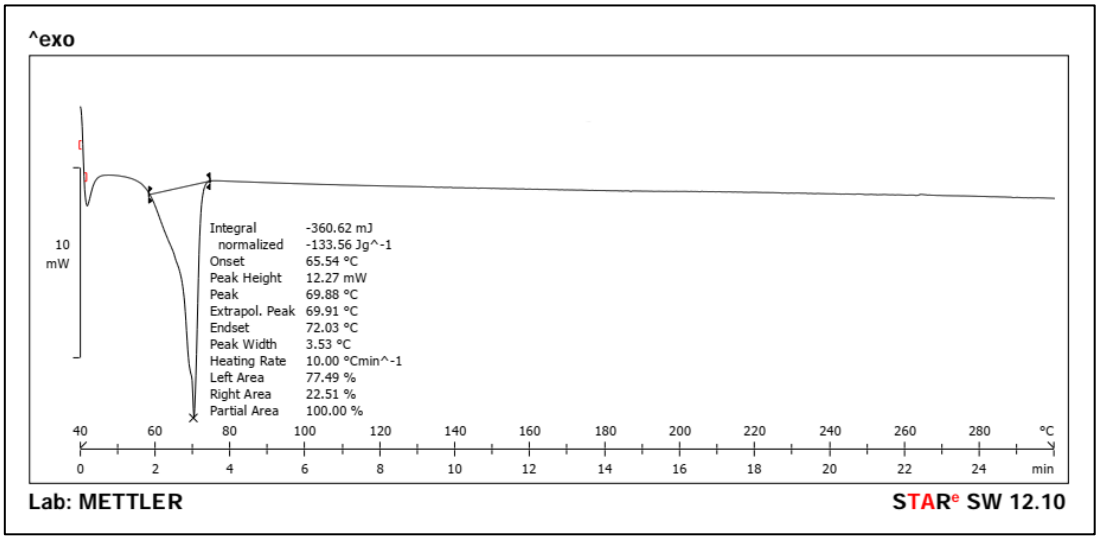

Figure 6: DSC Spectra of Allicin + Excipient

The Differential Scanning Calorimetry (DSC) analysis provides critical insights into the thermal behavior of Allicin both in its pure form and when combined with an excipient, essential for assessing drug-excipient compatibility. As depicted in Figure 5, the DSC spectrum of pure Allicin shows a sharp peak at 61.57°C, indicative of its melting point. This peak is characteristic of the thermal degradation point of Allicin, reflecting its inherent stability and purity. The clarity and sharpness of this peak in the DSC curve are vital benchmarks for comparing the thermal behavior of Allicin when formulated with excipients. Upon the introduction of an excipient, as shown in Figure 6, the DSC spectrum of the Allicin-excipient mixture exhibits a new peak at 69.88°C. The shift from 61.57°C to 69.88°C in the presence of the excipient suggests a change in the thermal properties of the drug. However, the absence of any additional unexpected peaks or significant broadening of the peak indicates no chemical interaction between Allicin and the excipient. This shift could be attributed to physical interactions such as dilution, altered crystallinity, or improved dispersion within the matrix, which are common in pharmaceutical formulations and do not necessarily indicate instability or incompatibility. Thus, the DSC results suggest that the excipient used does not adversely affect the thermal stability of Allicin, pointing towards a compatible drug-excipient relationship that is conducive to further formulation development.

3.6. Evaluation of Prepared formulations

Table 5: Summary of physicochemical parameters of prepared NS formulations

Formulation code	Particle size (nm)	Zeta potential (mV)	Entrapment efficiency (%)
PF1	222.76±2.87	-13.3	65.3±2.65
PF2	277.44±1.54	-15.5	61.6±3.54
PF3	361.27±2.34	-18.4	69.4±4.76
PF4	277.64±2.52	-19.3	67.8±5.44
PF5	331.49±2.28	-11.5	68.3±3.63
PF6	341.46±3.93	-16.8	63.3±4.43
PF7	273.52±3.28	-15.3	82.4±5.38
PF8	201.61±2.35	-12.8	58.9±2.32
PF9	332.42±1.82	-17.4	62.4±3.23

The evaluation of the physicochemical parameters of prepared nanosponge (NS) formulations, as summarized in Table 5, reveals a comprehensive insight into the attributes that dictate their potential efficacy and stability as drug delivery systems. These parameters include particle size, zeta potential, and entrapment efficiency, each contributing uniquely to the performance of the nanosponge formulations. The particle size across the formulations ranges from 201.61 nm to 361.27 nm, indicating a moderate variability in the size of the nanosponges, which can influence the release rate and penetration of the active pharmaceutical ingredients. Smaller particles, as observed in formulation PF8 (201.61±2.35 nm), typically exhibit higher surface area to volume ratios, potentially enhancing the dissolution rate and bioavailability of the drug. Conversely, larger particles, like those seen in formulation PF3 (361.27±2.34 nm), may favor slower release rates, which could be advantageous for sustained-release formulations.
Zeta potential values across the formulations range from -11.5 mV to -19.3 mV, which are indicative of moderate to good stability in colloidal systems. The negative values suggest that the particles are likely to repel each other, minimizing the risk of aggregation. Higher absolute

values of zeta potential, such as -19.3 mV seen in formulation PF4, generally suggest better stability, which is crucial for ensuring consistent drug delivery and shelf life. Entrapment efficiency is another critical parameter, with values ranging from 58.9% to 82.4%. Higher entrapment efficiencies, as seen in formulation PF7 (82.4±5.38%), suggest more effective incorporation of the drug into the nanosponges, which is beneficial for maximizing the therapeutic effect while minimizing the required dosage. Lower entrapment efficiencies, such as 58.9% in formulation F8, might indicate less efficient drug loading or potential leakage during the formulation process, which could affect the drug delivery efficacy. The variations in these parameters across the different formulations underscore the importance of optimizing the NS formulation to achieve the desired balance of stability, drug release, and efficacy. Such optimization could involve adjusting the polymer composition, cross-linking density, or the manufacturing process to tailor the nanosponges' characteristics to specific therapeutic needs.

3.7. Optimization of the Concentrations of Polyvinyl alcohol and Ethyl cellulose using Central composite design.

3.7.1. Effect of Formulation Variables on Entrapment Efficiency (R1)

Entrapment efficiency (R2) = +8544 +0.0100**A* -0.0233**B* +0.0575**AB* -0.0767A^2 +0.0233*B^2……. (2)

The optimization of the concentrations of Polyvinyl Alcohol (PVA) and Ethyl Cellulose (EC) using the Central Composite Design (CCD) and the subsequent ANOVA for the quadratic model for Entrapment Efficiency (R1) reveal insightful findings on the influence of these polymers on the entrapment efficiency of the formulation. The results, as detailed in Table 9.6, indicate a significant model with an F-value of 11.36 and a p-value of 0.0365, suggesting that the model is statistically significant for predicting the entrapment efficiency of the nanosponge formulations. The individual effects of PVA and EC, denoted as A and B respectively, show differing impacts on entrapment efficiency. The p-value for PVA (A) is 0.0959, which borders on significance, suggesting that PVA has a noticeable but not dominant effect on the entrapment efficiency. This is also reflected in the regression equation, where the coefficient for A is positive but small (0.0100), indicating a slight increase in entrapment efficiency with higher concentrations of PVA. In contrast, EC (B) has a much smaller and statistically insignificant effect (p-value = 0.8544) with a negative coefficient (-0.0233) in the regression equation, suggesting that increasing levels of EC might slightly decrease entrapment efficiency, although this effect is minimal.

The interaction term (AB) and the quadratic terms (A^2 and B^2) provide additional insights. The interaction between PVA and EC (AB) has a p-value of 0.5466, showing that their interaction is not significant and does not substantially influence entrapment efficiency. However, the quadratic terms show significant effects; particularly, the term for EC (B^2) has a very significant p-value (0.0058) and a positive coefficient (0.0233), indicating that the relationship between EC concentration and entrapment efficiency is parabolic and increases at higher levels. This suggests that while low to moderate increases in EC concentration might not affect or decrease entrapment efficiency, higher concentrations significantly enhance it. The regression analysis corroborate these findings, where the R^2 value of 0.9498 demonstrates that the model explains a high proportion of the variability in entrapment efficiency. However, the adjusted R^2 of 0.8662, while still high, indicates some overfitting when all predictors are considered. The Adequate Precision value of 10.2880 shows an adequate signal-to-noise ratio, supporting the model's use in navigating the design space. The optimization and analysis suggest that while

both PVA and EC influence the entrapment efficiency of the nanosponge formulations, the effects of EC, especially at higher concentrations, are more pronounced. These results provide a foundation for further refining polymer concentrations in nanosponge formulations to achieve optimal drug entrapment.

The comprehensive analysis and optimization of the concentrations of Polyvinyl Alcohol (PVA) and Ethyl Cellulose (EC) using Central Composite Design (CCD) have yielded significant insights into the formulation variables affecting the entrapment efficiency of nanosponges. Figures 7a and 7b illustrate the contour and 3D response surface plots, respectively, demonstrating the interaction between PVA and EC and their impact on the entrapment efficiency. These graphical representations highlight the optimum regions where both polymers synergistically enhance the entrapment efficiency, revealing a peak efficiency

at specific concentrations of both PVA and EC. Figure 7a (Contour plot) and Figure 7b (3D surface plot), it is apparent that the entrapment efficiency reaches its peak when PVA and EC are used in certain optimal ratios. This is particularly evident in the central regions of these plots, where the entrapment efficiency significantly increases as indicated by the warmer color tones in the contour plot and the peak in the 3D surface plot. This suggests that there is an optimal balance of polymer concentrations that maximizes the drug's entrapment within the nanosponge matrix, likely due to the complementary physical and chemical properties of the polymers that enhance matrix stability and drug-polymer interaction.

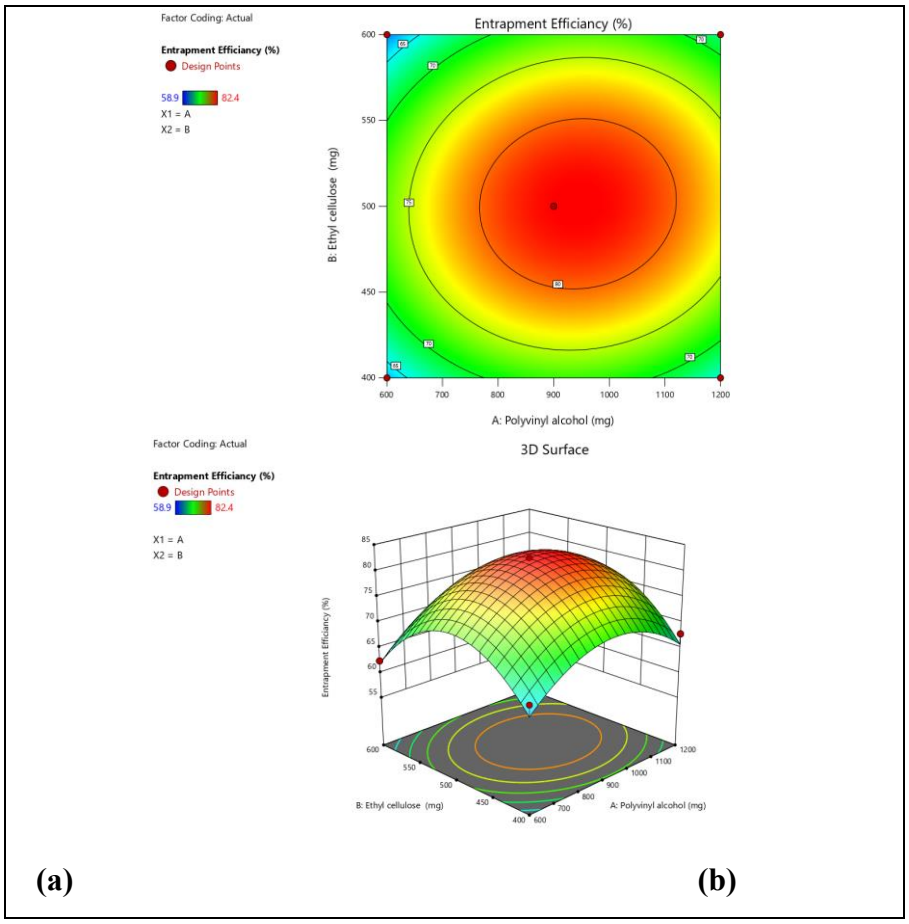

Figure 7: Contour plot (a) and 3D surface plot (b) presenting the interaction between the Polyvinyl alcohol and Ethyl cellulose affecting Entrapment efficiency (R1)

3.7.2. Effect of Formulation Variables on Particle size (R1)

$$\text{Particle size} = +8544 + 0.0100*A - 0.0233*B + 0.0575*AB - 0.0767A^2 + 0.0233*B^2 \quad (3)$$

The ANOVA results for the quadratic model regarding the particle size of the formulations as depicted in Table 6 clearly illustrate the significant impact of the formulation variables, particularly Ethyl Cellulose (EC), on the particle size of nanosponges. The model itself is statistically significant, as evidenced by an F-value of 27.38 and a p-value of 0.0105, indicating that the model is robust and capable of predicting the particle size based on the given inputs of Polyvinyl Alcohol (PVA) and EC. analyzing the individual contributions, the effect of EC (B) on particle size is particularly noteworthy with an F-value of 53.07 and a p-value of 0.0053, suggesting a very strong influence of EC on increasing particle size. This could be due to the physicochemical properties of EC, which may increase the viscosity of the solution, thereby leading to larger particle formation during the nanosponges synthesis. In contrast, the influence of PVA (A) and the interaction term (AB) are not statistically significant (p-values of 0.1146 and 0.1238, respectively), indicating that their effects on particle size are less pronounced compared to EC. The quadratic terms (A^2 and B^2) also indicate significant effects, with A^2 showing a notable impact with a p-value of 0.0162. This suggests a non-linear relationship where variations in PVA concentrations can lead to different impacts on particle size at different levels of addition.

The curvature in the response surface, as indicated by the significant A^2 term, points to the complex interplay of PVA in the formulation matrix affecting particle size. The regression analysis further validates the robustness of the model with an R^2 value of 0.9786, suggesting that 97.86% of the variability in particle size can be explained by the model. The Adjusted R^2 value of 0.9428 reaffirms that the model is highly predictive within the design space and the Adequate Precision ratio of 16.2354 indicates an adequate signal. This model can, therefore, be reliably used to navigate the design space for optimal formulation. The statistical analysis and the resulting regression model provide a deep insight into how both PVA and particularly EC affect the particle size of the nanosponges. It highlights the dominance of EC in controlling particle size, potentially guiding further optimization strategies for tailoring nanosponge properties for specific application needs. Such insights are crucial for developing effective and efficient drug delivery systems using nanosponge technology.

The comprehensive analysis of particle size optimization using a Central Composite Design (CCD) reveals the profound impact of both Polyvinyl Alcohol (PVA) and Ethyl Cellulose (EC) on the particle size of the formulations. As evidenced by the contour and 3D response surface plots (Figures 8a and 8b), the interplay between these two polymers significantly influences particle size, offering critical insights into how each component affects the final properties of the nanosponges. In the contour plot (Figure 8a), the gradient of colors indicates varying particle sizes across different concentrations of PVA and EC. The green-to-yellow transition denotes an increase in particle size, suggesting that higher concentrations of PVA and/or EC generally lead to the formation of larger particles. This is corroborated by the 3D response surface plot (Figure 8b), which shows a clear peak, indicating that at certain concentrations of PVA and EC, particle size reaches a maximum. These plots are instrumental in pinpointing the optimal ratios of PVA and EC that balance particle size for desired release profiles and stability.

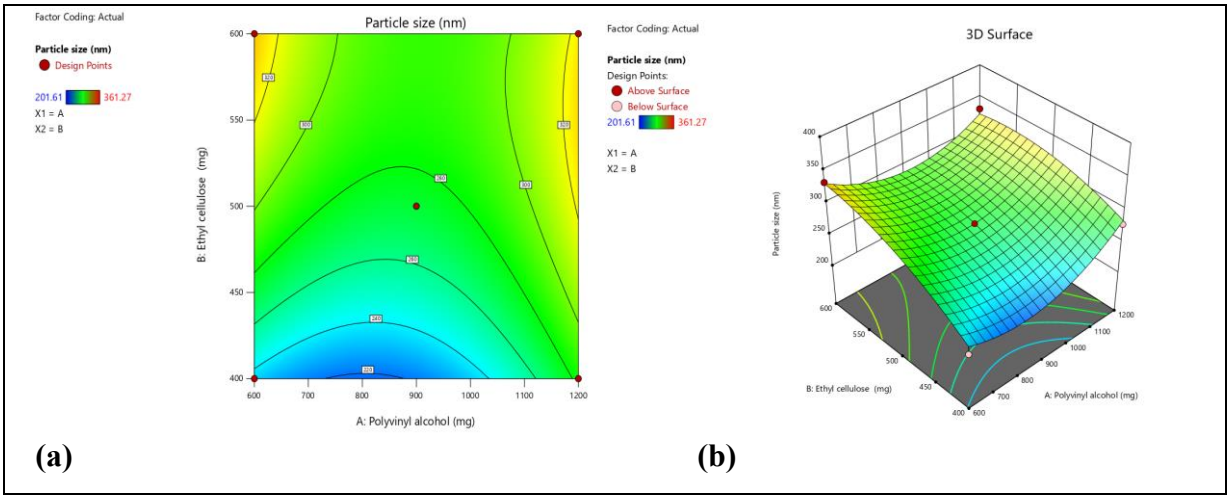

Figure 8: Contour plot (a) and 3D surface plot (b) presenting the interaction between the Polyvinyl alcohol and Ethyl cellulose affecting Particle size (R2)

3.7.3. Results of regression analysis

Table 6: ANOVA results for the quadratic model for the response Entrapment efficiency (R1) and Particle size (R2).

Response	Result value

Entrapment efficiency (R1)	
Sum of squares	357.44
Df	5
Mean square	71.49
F Value	11.36
P value	0.0365
R^2	0.9498
Adjusted R^2	0.8662
Predicted R^2	NA(1)
Std. Dev.	2.51
Mean	66.60
C.V. %	3.77
	Significant
Particle size (R2)	
Sum of squares	23636.27
Df	5
Mean square	4727.25
F Value	27.38
P value	0.0105
R^2	0.9786
Adjusted R^2	0.9428
Predicted R^2	NA(1)
Std. Dev.	13.14
Mean	291.07
C.V. %	4.51
	Significant

3.8. Optimization of Statistical Model.

The validation of the statistical model confirmed PF7 as the optimized batch. The experimental values for Entrapment efficiency and Particle size with the predicted values by Design-Expert software, as shown in Table 7, indicate the model's high accuracy. The minimal standard deviation in Entrapment efficiency and Particle size reinforces the reliability of the formulation process, establishing PF7 as the batch that meets the optimization criteria set by the study. The PF7 batch indicated as an optimized batch proved that the model was successfully validated.

Table 7: The predicted and experimental values of response variables and percentage error.

F. Code	**Composition**	**Response**	**Predicted value**	**Experimental value**	**Error Difference**
PF7	Polyvinyl alcohol Ethyl cellulose	Entrapment efficiency	82.4	82.4	0
PF7	Polyvinyl alcohol Ethyl cellulose	Particle size	281.3	273.5	7.8

3.9. *In-Vitro* release studies NS formulation

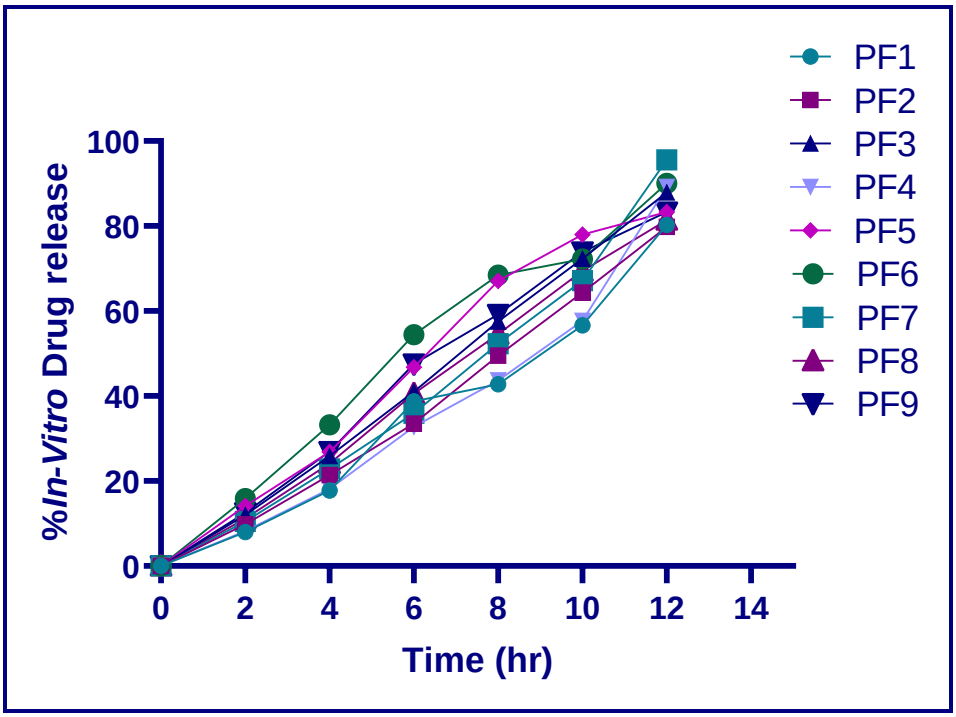

Figure 9: *In-vitro* drug release studies of NS

The *in-vitro* release studies of the nanosponge (NS) formulations, as presented, illustrate distinct release profiles across various formulations (PF1 to PF9) over a 12-hour period. Initial observations at the 2-hour mark reveal a gradual commencement in drug release, with PF6 showing the highest release at 15.89%, suggesting a quicker initial release rate, which could be advantageous for conditions requiring rapid onset of action. PF1, on the other hand, shows the least release at 8.02%, indicating a slower release mechanism that might be preferable for prolonged therapeutic effects. The variance in release rates could be attributed to differences in formulation compositions, possibly including variations in polymer ratios, particle size, or even the physical stability of the nanosponge matrix. As the time progresses to 12 hours, all formulations show significant increases in drug release, with PF7 exhibiting an exceptionally high release rate at 95.57%, which suggests a nearly complete drug release profile. This could indicate a less robust matrix allowing for faster drug diffusion. In contrast, PF1 and PF8, while showing substantial release improvements, still retain lower overall release percentages (80.25% and 81.39% respectively), highlighting their potential for sustained release applications. The consistent increase in drug release rates across all formulations by the end of the 12-hour period demonstrates the effectiveness of the NS system in maintaining a controlled release, yet the differences in the extent of release at each time point underscore the impact of formulation nuances on the release dynamics. These results are crucial for tailoring NS formulations to specific therapeutic needs, balancing between rapid and sustained release as required by the treatment regimen.

3.10. Characterization of Nanosponges loaded gel. (Optimized Batch-PF7)

Table 8: Results of the characterization of the NS loaded Gel formulation of allicin.

Batch	Color	Appearance	Odor	**pH**	**Spreadability (gm. cm/sec)**	**Viscosity (cps)**

GF	Greenish Brown	Clear, Thick	Odourless	6.7±0.09	12.2±0.78	4425±33.64

The characterization of the optimized nanosponge-loaded gel formulation of allicin (Table 8), designated as batch GF, reveals several key physicochemical properties critical for its potential therapeutic application and patient acceptability. The gel is described as having a greenish-brown color and a clear, thick appearance, which are important for ensuring uniformity and aesthetic acceptance by users. The absence of odor is a beneficial attribute, especially for a product intended for potentially sensitive applications, as it enhances the likelihood of adherence to treatment by patients who may be sensitive to strong or medicinal smells. From a functional standpoint, the pH of the gel is recorded at 6.7±0.09, which is close to neutral. This pH level is particularly advantageous for topical applications as it is likely to be non-irritating and compatible with the skin's natural pH, minimizing the risk of irritation or discomfort upon application. The spreadability of the gel, measured at 12.2±0.78 gm. cm/sec, indicates good physical handling characteristics, suggesting that the gel can be easily and evenly applied to the skin, allowing for efficient drug delivery over the intended area. Additionally, the viscosity of 4425±33.64 cps implies that the gel possesses sufficient thickness to remain in place after application, preventing runoff and ensuring that the drug remains at the site of application for effective absorption.

3.11. Results of *In-vitro* antifungal activity

Table 9: *In-vitro* antifungal activity of allicin, GF and Marketed Standard.

Sr. No.	**Name of Sample**	**Zone of Inhibition (mm)***	
		Candida albicans	***Aspergillus Niger***
1.	Allicin	24.3±0.76	25.2±0.32
2.	GF (NS (PF7) loaded gel)	23.5±0.87	24.4±1.23
3.	Marketed standard	26.7±0.78	24.3±0.67

Values are expressed in mean±SD, (n =3).

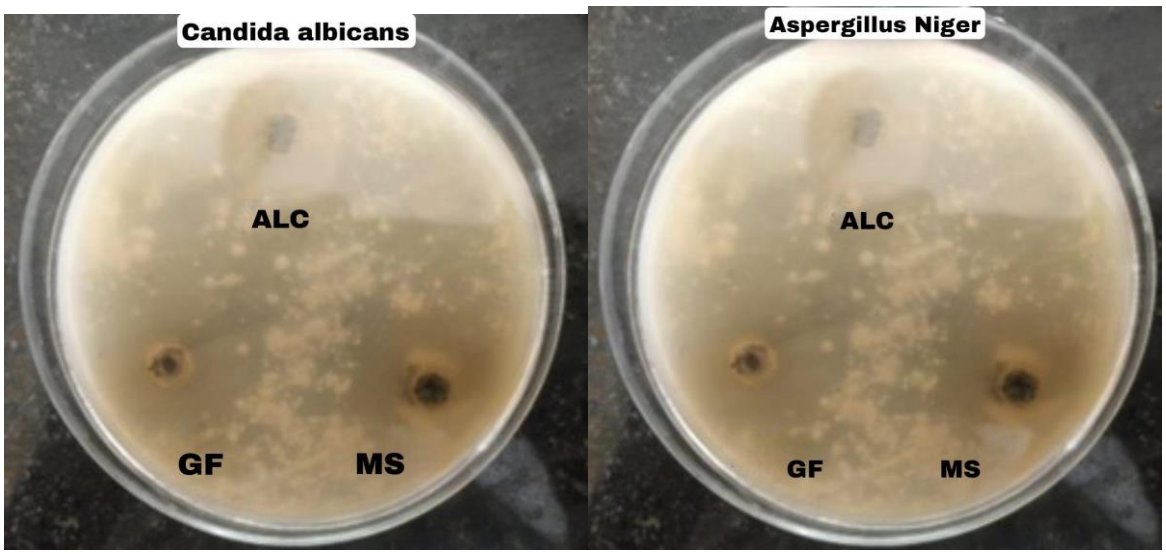

Figure 10: Zone of Inhibition of *In-vitro* antifungal activity of Allicin (ALC), GF (NS (PF7) loaded gel) and marketed standard.

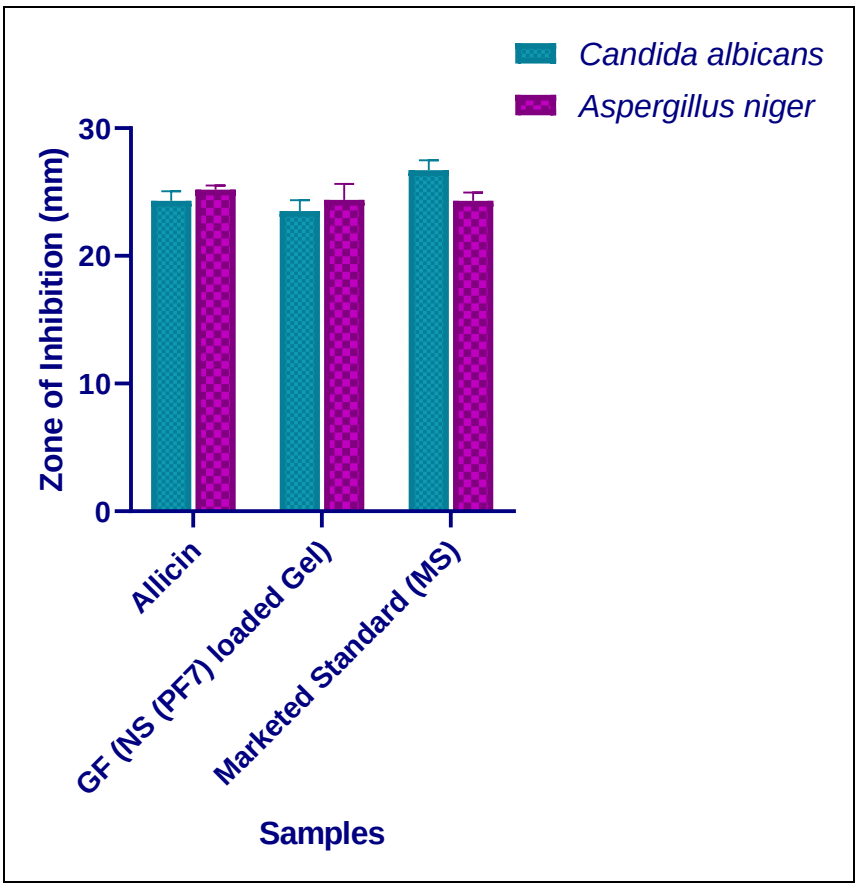

Figure 11: Graphical representation of the *In-vitro* antifungal activity of allicin, GF (NS (PF7) loaded gel) and Marketed standard (MS).

The *in-vitro* antifungal activity results for allicin, the optimized nanosponge-loaded gel (GF), and a marketed standard, as summarized in Table 9 and depicted in Figures 10 and 11, provide insightful comparisons into their efficacy against two common fungal pathogens: *Candida albicans* and *Aspergillus niger*. The zone of inhibition measurements serve as a direct indicator of antifungal effectiveness, with larger zones correlating to greater antifungal activity. Allicin shows significant antifungal activity with zones of inhibition measuring 24.3±0.76 mm against *Candida albicans* and 25.2±0.32 mm against *Aspergillus niger*. These results are indicative of allicin's strong inherent antifungal properties. The GF (NS (PF7) loaded gel), which contains the optimized nanosponge formulation of allicin, similarly exhibits substantial antifungal effectiveness, though slightly lower than pure allicin, with inhibition zones of 23.5±0.87 mm against *Candida albicans* and 24.4±1.23 mm against *Aspergillus niger*. The slight reduction in the zone of inhibition for the gel formulation could be attributed to the controlled release properties of the nanosponge matrix, which may release allicin at a slower rate compared to its pure form.

The marketed standard displays a varied pattern of inhibition, with a zone of 26.7±0.78 mm against *Candida albicans*, which is the highest among the samples, and 24.3±0.67 mm against *Aspergillus niger*, which is comparable to allicin and slightly lower than its performance against *Candida albicans*. This suggests that while the marketed standard is highly effective, particularly against *Candida albicans*, the GF gel holds its own in terms of efficacy, providing a nearly equivalent antifungal capability, which is notable given its formulation advantages

such as enhanced application properties and potential for improved patient compliance. Overall, these results underscore the effectiveness of the nanosponge formulation in maintaining the antifungal activity of allicin while also providing additional benefits in terms of application and release characteristics. This makes GF an attractive alternative to both the pure compound and existing market formulations, offering a balanced combination of efficacy and usability for antifungal treatment applications.

4. Conclusion

The present study successfully developed and fabricated a nanosponge-loaded gel formulation of allicin for the treatment of topical fungal infections, demonstrating its potential as an effective therapeutic option. The calibration curve of allicin in ethanol showed a high correlation coefficient, confirming the reliability of the method used. Solubility analysis revealed that allicin has higher solubility in organic solvents compared to water, which is advantageous for non-aqueous formulations. The melting point and FTIR analyses confirmed the stability and compatibility of allicin with the selected excipients. DSC analysis indicated no significant interaction between allicin and the excipients, ensuring the thermal stability of the formulation. The evaluation of physicochemical parameters highlighted the optimized formulation with desirable particle size, zeta potential, and entrapment efficiency. Optimization using central composite design identified the best ratios of polyvinyl alcohol and ethyl cellulose for maximizing entrapment efficiency and controlling particle size. In-vitro release studies demonstrated a controlled release profile, and the optimized nanosponge-loaded gel (GF) exhibited substantial antifungal activity comparable to a marketed standard, underscoring its potential as an effective and user-friendly topical antifungal treatment.

Abbreviations
ANOVA: Anova of Variance; FTIR: Fourier-transform infrared spectroscopy; DSC: Differential scanning calorimetry; UV: Ultra-violet spectroscopy; Df: Degree of freedom; GF: Gel formulation; PVA: Polyvinyl alcohol; EC: Ethyl Cellulose; NS: Nanosponges.

Acknowledgement
The authors would like to acknowledge the support and guidance of Principal [Name of Principal], [College Name] provided in conducting this research. His constant encouragement and valuable suggestions were instrumental in completing this study. The authors also thank Sciquaint Innovations (OPC) Private Limited, Pune, India, for providing the of allicin to carry out this research.

Conflict of Interest
Authors declares that there is no conflict of Interest.

Author Contributions
All author contributed equally.

5. References

1. D. A. Enoch, H. Yang, S. H. Aliyu, and C. Micallef, “The Changing Epidemiology of Invasive Fungal Infections,” in *Human Fungal Pathogen Identification: Methods and*

Protocols, T. Lion, Ed., New York, NY: Springer, 2017, pp. 17–65. doi: 10.1007/978-1-4939-6515-1_2.
2. M. von Lilienfeld-Toal, J. Wagener, H. Einsele, O. A. Cornely, and O. Kurzai, "Invasive Fungal Infection," *Dtsch. Ärztebl. Int.*, vol. 116, no. 16, pp. 271–278, Apr. 2019, doi: 10.3238/arztebl.2019.0271.
3. D. Z. P. Friedman and I. S. Schwartz, "Emerging Fungal Infections: New Patients, New Patterns, and New Pathogens," *J. Fungi*, vol. 5, no. 3, Art. no. 3, Sep. 2019, doi: 10.3390/jof5030067.
4. S. Seyedmousavi *et al.*, "Fungal infections in animals: a patchwork of different situations," *Med. Mycol.*, vol. 56, no. suppl_1, pp. S165–S187, Apr. 2018, doi: 10.1093/mmy/myx104.
5. K. Kainz, M. A. Bauer, F. Madeo, and D. Carmona-Gutierrez, "Fungal infections in humans: the silent crisis," *Microb. Cell*, vol. 7, no. 6, pp. 143–145, doi: 10.15698/mic2020.06.718.
6. B. Salehi *et al.*, "Allicin and health: A comprehensive review," *Trends Food Sci. Technol.*, vol. 86, pp. 502–516, Apr. 2019, doi: 10.1016/j.tifs.2019.03.003.
7. J. Reiter, A. M. Hübbers, F. Albrecht, L. I. O. Leichert, and A. J. Slusarenko, "Allicin, a natural antimicrobial defence substance from garlic, inhibits DNA gyrase activity in bacteria," *Int. J. Med. Microbiol.*, vol. 310, no. 1, p. 151359, Jan. 2020, doi: 10.1016/j.ijmm.2019.151359.
8. Y. Zhou *et al.*, "Allicin in Digestive System Cancer: From Biological Effects to Clinical Treatment," *Front. Pharmacol.*, vol. 13, Jun. 2022, doi: 10.3389/fphar.2022.903259.
9. A. Marchese *et al.*, "Antifungal and antibacterial activities of allicin: A review," *Trends Food Sci. Technol.*, vol. 52, pp. 49–56, Jun. 2016, doi: 10.1016/j.tifs.2016.03.010.
10. J. G. Sheppard, J. P. McAleer, P. Saralkar, W. J. Geldenhuys, and T. E. Long, "Allicin-inspired pyridyl disulfides as antimicrobial agents for multidrug-resistant *Staphylococcus aureus*," *Eur. J. Med. Chem.*, vol. 143, pp. 1185–1195, Jan. 2018, doi: 10.1016/j.ejmech.2017.10.018.
11. M. Nakamoto, K. Kunimura, J.-I. Suzuki, and Y. Kodera, "Antimicrobial properties of hydrophobic compounds in garlic: Allicin, vinyldithiin, ajoene and diallyl polysulfides (Review)," *Exp. Ther. Med.*, vol. 19, no. 2, pp. 1550–1553, Feb. 2020, doi: 10.3892/etm.2019.8388.
12. S. Xu, Y. Liao, Q. Wang, L. Liu, and W. Yang, "Current studies and potential future research directions on biological effects and related mechanisms of allicin," *Crit. Rev. Food Sci. Nutr.*, vol. 63, no. 25, pp. 7722–7748, Oct. 2023, doi: 10.1080/10408398.2022.2049691.
13. S. Wang, D. Wang, Y. Duan, Z. Zhou, W. Gao, and L. Zhang, "Cellular Nanosponges for Biological Neutralization," *Adv. Mater.*, vol. 34, no. 13, p. 2107719, 2022, doi: 10.1002/adma.202107719.
14. A. P. Sherje, B. R. Dravyakar, D. Kadam, and M. Jadhav, "Cyclodextrin-based nanosponges: A critical review," *Carbohydr. Polym.*, vol. 173, pp. 37–49, Oct. 2017, doi: 10.1016/j.carbpol.2017.05.086.
15. K. Tiwari and S. Bhattacharya, "The ascension of nanosponges as a drug delivery carrier: preparation, characterization, and applications," *J. Mater. Sci. Mater. Med.*, vol. 33, no. 3, p. 28, Mar. 2022, doi: 10.1007/s10856-022-06652-9.

16. S. Swaminathan, R. Cavalli, and F. Trotta, "Cyclodextrin-based nanosponges: a versatile platform for cancer nanotherapeutics development," *WIREs Nanomedicine Nanobiotechnology*, vol. 8, no. 4, pp. 579–601, 2016, doi: 10.1002/wnan.1384.
17. A. Garg *et al.*, "Nanosponge: A promising and intriguing strategy in medical and pharmaceutical Science," *Heliyon*, vol. 10, no. 1, p. e23303, Jan. 2024, doi: 10.1016/j.heliyon.2023.e23303.
18. F. Caldera, M. Tannous, R. Cavalli, M. Zanetti, and F. Trotta, "Evolution of Cyclodextrin Nanosponges," *Int. J. Pharm.*, vol. 531, no. 2, pp. 470–479, Oct. 2017, doi: 10.1016/j.ijpharm.2017.06.072.
19. S. Iravani and R. S. Varma, "Nanosponges for Drug Delivery and Cancer Therapy: Recent Advances," *Nanomaterials*, vol. 12, no. 14, Jul. 2022, doi: 10.3390/nano12142440.
20. Y. Nait Bachir, M. Medjekane, F. Benaoudj, naima sahraoui, and H. Ziane-Zafour, "Formulation of β-Cyclodextrin Nanosponges by Polycondensation Method: Application for Natural Drugs Delivery and Preservation," *J. Mater. Process. Environ.*, vol. 5, pp. 81–85, Jun. 2017.
21. D. A. Gaber *et al.*, "Formulation and evaluation of Piroxicam nanosponge for improved internal solubility and analgesic activity," *Drug Deliv.*, vol. 30, no. 1, p. 2174208, Dec. 2023, doi: 10.1080/10717544.2023.2174208.
22. K. V. Sri, G. Santhoshini, D. R. Sankar, and K.Niharika, "Formulation and Evaluation of Rutin Loaded Nanosponges," *Asian J. Res. Pharm. Sci.*, vol. 8, no. 1, pp. 21–24, Mar. 2018, doi: 10.5958/2231-5659.2018.00005.X.
23. Pushpalatha D, Abdul Waris Khan, Manjunath K, and Brunda S, "Formulation and evaluation of lovastatin loaded nanosponges," *World J. Adv. Res. Rev.*, vol. 11, no. 3, pp. 041–056, Sep. 2021, doi: 10.30574/wjarr.2021.11.3.0404.
24. S. P.r., N. R. James, A. kumar P.r., and D. K. Raj, "Preparation, characterization and biological evaluation of curcumin loaded alginate aldehyde–gelatin nanogels," *Mater. Sci. Eng. C*, vol. 68, pp. 251–257, Nov. 2016, doi: 10.1016/j.msec.2016.05.046.
25. S. M. Omar, F. Ibrahim, and A. Ismail, "Formulation and evaluation of cyclodextrin-based nanosponges of griseofulvin as pediatric oral liquid dosage form for enhancing bioavailability and masking bitter taste," *Saudi Pharm. J.*, vol. 28, no. 3, pp. 349–361, Mar. 2020, doi: 10.1016/j.jsps.2020.01.016.
26. M. M. Ahmed, F. Fatima, M. K. Anwer, M. J. Ansari, S. S. Das, and S. M. Alshahrani, "Development and characterization of ethyl cellulose nanosponges for sustained release of brigatinib for the treatment of non-small cell lung cancer," *J. Polym. Eng.*, vol. 40, no. 10, pp. 823–832, Nov. 2020, doi: 10.1515/polyeng-2019-0365.
27. S. Allahyari *et al.*, "Preparation and characterization of cyclodextrin nanosponges for bortezomib delivery," *Expert Opin. Drug Deliv.*, vol. 17, no. 12, pp. 1807–1816, Dec. 2020, doi: 10.1080/17425247.2020.1800637.
28. S. El-Housiny *et al.*, "Fluconazole-loaded solid lipid nanoparticles topical gel for treatment of pityriasis versicolor: formulation and clinical study," *Drug Deliv.*, vol. 25, no. 1, pp. 78–90, Jan. 2018, doi: 10.1080/10717544.2017.1413444.
29. H. V. Gangadharappa, S. M. Chandra Prasad, and R. P. Singh, "Formulation, *in vitro* and *in vivo* evaluation of celecoxib nanosponge hydrogels for topical application," *J. Drug Deliv. Sci. Technol.*, vol. 41, pp. 488–501, Oct. 2017, doi: 10.1016/j.jddst.2017.09.004.
30. E. Dingwoke and S. Y. Felix, "DEVELOPMENT AND EVALUATION OF NANOSPONGES LOADED EXTENDED RELEASE TABLETS OF LANSOPRAZOLE," *Univers. J. Pharm. Res.*, Mar. 2019, doi: 10.22270/ujpr.v4i1.239.

31. P. O. Nnamani *et al.*, "Formulation and evaluation of transdermal nanogel for delivery of artemether," *Drug Deliv. Transl. Res.*, vol. 11, no. 4, pp. 1655–1674, Aug. 2021, doi: 10.1007/s13346-021-00951-4.
32. G. K. Saraogi *et al.*, "Formulation Development and Evaluation of Pravastatin-Loaded Nanogel for Hyperlipidemia Management," *Gels*, vol. 8, no. 2, Art. no. 2, Feb. 2022, doi: 10.3390/gels8020081.
33. V. Avasatthi, H. Pawar, C. P. Dora, P. Bansod, M. S. Gill, and S. Suresh, "A novel nanogel formulation of methotrexate for topical treatment of psoriasis: optimization, in vitro and in vivo evaluation," *Pharm. Dev. Technol.*, vol. 21, no. 5, pp. 554–562, Jul. 2016, doi: 10.3109/10837450.2015.1026605.
34. M. D. C. Sales, H. B. Costa, P. M. B. Fernandes, J. A. Ventura, and D. D. Meira, "Antifungal activity of plant extracts with potential to control plant pathogens in pineapple," *Asian Pac. J. Trop. Biomed.*, vol. 6, no. 1, pp. 26–31, Jan. 2016, doi: 10.1016/j.apjtb.2015.09.026.
35. S. Manandhar, S. Luitel, and R. K. Dahal, "In Vitro Antimicrobial Activity of Some Medicinal Plants against Human Pathogenic Bacteria," *J. Trop. Med.*, vol. 2019, p. e1895340, Apr. 2019, doi: 10.1155/2019/1895340.